ORIGINAL RESEARCH PAPER

Applying wavelet transform to suppress ghost in ocean-bottom node dual-sensor technology

Xiawan Zhou[1] · Peng Guo[2] · Sha Song[1] · Qingchun Li[1]

Abstract

In ocean-bottom node (OBN) seismic exploration, a ghost is a common interference wave that affects the accuracy of seismic data interpretation. Receiver de-ghosting can be achieved using dual-sensor summation technology, which employs a hydrophone and geophone to collect seismic signals. The differences between the two receivers cause the polarities of the ghost wave signals to be opposite; therefore, the ghost waves can be eliminated by adding these receivers. However, there are differences between the actual data obtained from the hydrophone and geophone with regard to frequency, phase, and amplitude, thereby preventing them from being directly summated. Therefore, the frequency, phase and amplitude of both data records must be matched for consistency before dual-sensor summation can be conducted. In addition, some noise and ghosts will remain during data processing, resulting in a reduction in the signal-to-noise ratio of the data, making it necessary to adopt noise and residual ghost suppression methods. In this study, a wavelet analysis was newly introduced to the dual-sensor summation process. Specifically, the wavelet spectrum whitening method was proposed for the frequency matching of dual-sensor data, and the nonlinear wavelet transform threshold method of the wavelet denoising method was applied to suppress the noise and residual ghost. On this basis, a new dual-sensor process flow in OBN seismic exploration was developed. The feasibility and effectiveness of the method were verified using actual data. The method proposed in this study will help to improve the accuracy of future data processing.

Introduction

In ocean bottom nodes (OBN) seismic prospecting, a source is located near the sea surface, while geophones are usually placed below the sea surface or on the seabed. The sea surface can be used as a reflector, but its reflection coefficient

✉ Qingchun Li
  dcliqc@chd.edu.cn

  Xiawan Zhou
  zxw13299118153@163.com

  Peng Guo
  18215466159@163.com

  Sha Song
  shasong@chd.edu.cn

[1] College of Geological Engineering and Geomatics, Chang'an University, Xi'an 710054, China

[2] School of Water and Environment, Chang'an University, Xi'an 710054, China

is large, generally regarded as − 1. Thus, in addition to the effective waves that are reflected from the seafloor interface, the descending waves (Fig. 1) reflected from the sea level are also collected. These descending waves are called ghosts (reverberations). A ghost follows the effective wave, interfering with the effective wave and occasionally forming a false in-phase axis. Therefore, a ghost can significantly impact signal resolution. In addition, based on the frequency spectrum, the notch effect caused by the ghost can cause some frequency bands in the effective wave to disappear, thereby weakening the energy of the effective signal (Fig. 2). Therefore, suppressing the impact of the ghost in seismic exploration data is an indispensable step in seismic data processing.

Several methods exist to suppress the ghost, among which dual-sensor synthesis technology is the most commonly used, suppressing the ghost at the receiving end. In 1989, Barr and Sanders first proposed eliminating the ghost in seismic records by using the dual-sensor receiving technology. They found that the ghost in the records can be eliminated by
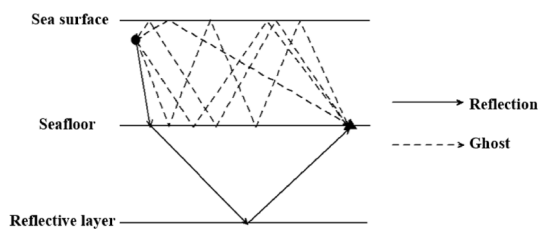
Fig. 1 Ghost path

combining the records, as the polarity of ghost recorded by pressure (hydrophone) and velocity detectors (geophone) is opposite. However, the internal structure, working principle, and the type of signal received by the pressure and velocity detectors are different, causing them to vary in frequency, amplitude, and phase, preventing their direct synthesis.

Therefore, the key of dual-sensor synthesis technology is to process the dual-sensor data to ensure that the two can reach the same frequency, amplitude, and phase.

The difference in amplitude between the dual-sensor data is the most distinct, usually varying by several orders of magnitude. Therefore, amplitude matching needs to be performed prior to dual-sensor combination processing (Ball and Corrigan 1996). When a seismic wave is perpendicular incident, the proportional factor of the amplitude between the geophone and hydrophone records is $(1 + Kr)/(1 − Kr)$; here, Kr represents the sea bottom reflection coefficient (Barr and Sanders 1989), which can be further optimised to $\rho c(1 + Kr)/(1 − Kr)$, where ρ is the density of the sea water and c is the velocity of the sea water (Hoffe et al. 2000). For general seismic waves, the matching coefficient of the dual-sensor can be directly calculated using the average autocorrelation of the reflected
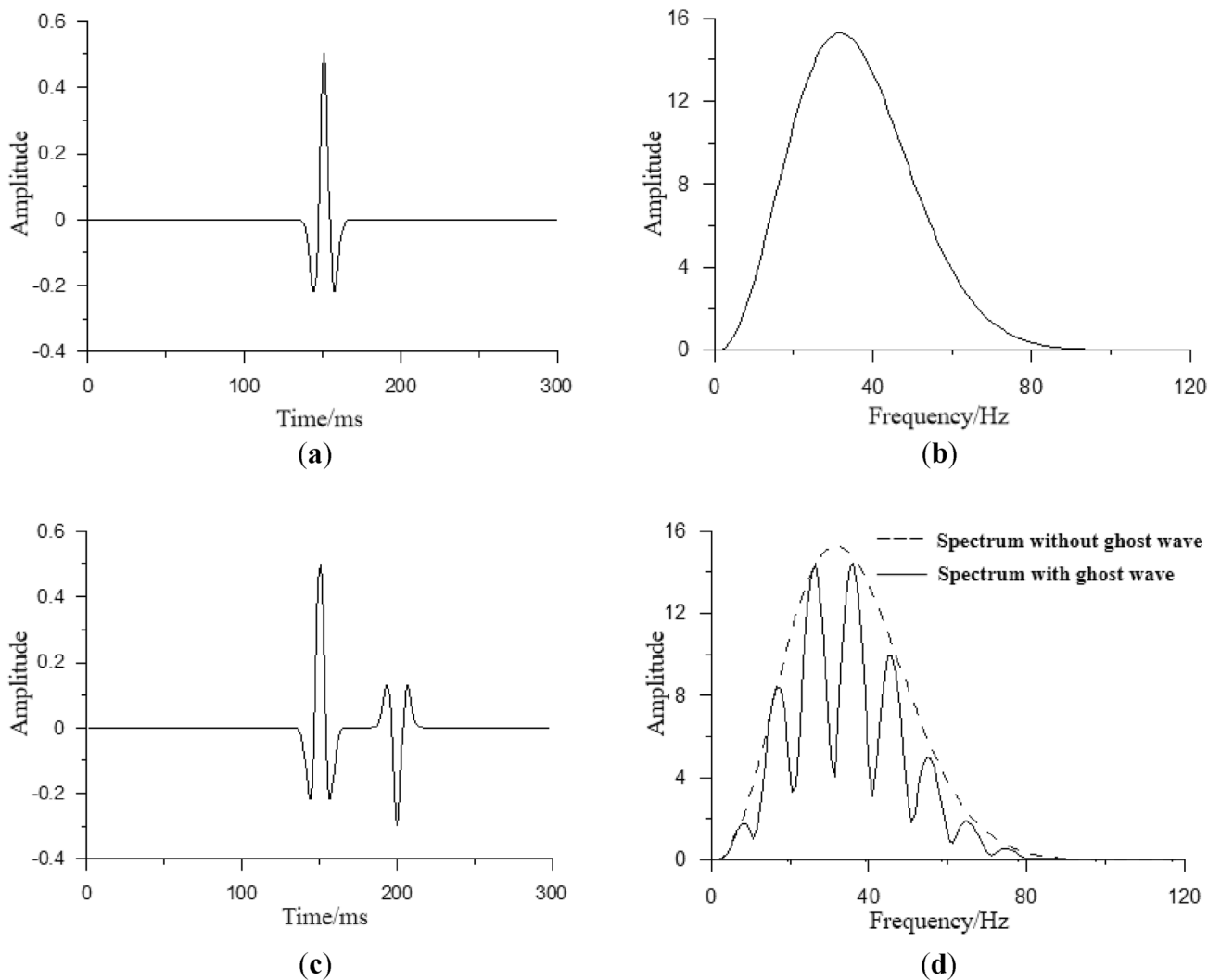

Fig. 2 Influence of ghost waves on the signal spectrum. **a** A single channel record with primary reflection only, **b** spectrum of the primary reflection wave, **c** single channel record with primary reflection and ghost wave, and **d** comparison of spectrum data with and without ghost waves

waves collected (Dragoset and Barr 1994). Based on the decomposition of the one-dimensional wave equation into the upward and downward waves, the bottom reflection coefficient can be effectively extracted directly from the original seismic data (Paffenholz and Barr 1995), or by obtaining statistics on the amplitude value of the seismic data of each channel to calculate the amplitude matching factor (Quan and Han 2005). The single-channel Wiener filtering method can also be used to obtain the amplitude matching coefficient of the hydrophone and geophone data (Tong et al. 2012), or the amplitude calibration factor can be calculated using the minimum energy as the criterion (Gao et al. 2015). Overall, amplitude matching methods are relatively mature and effective. In dual-sensor summations, the matching factor of phase is required as well (Ball and Corrigan 1996). The phase difference in the dual-sensor data is generally 90° (Song et al. 2004), and the phase correction method in terrestrial exploration can be adopted. In this regard, conventional processing uses a scanning method to determine the phase matching factor. That is, the phase matching factor range and scanning step length (Zhou 1989; Jiao et al. 1998; Ball and Corrigan 1996; Gao et al. 2001; Levy and Oldenburg 1987) are pre-set, after which a scanning method is used to give a series of phase matching factor values. Then, the cross-correlation function of the dual-senor is determined, using which the maximum energy is calculated. Subsequently, the best phase matching factor is derived from the maximum energy. In this scenario, the similarity coefficient criterion in the constant phase correction is introduced into the dual-sensor phase matching, which not only enables a faster calculation speed but also provides a better matching effect (Tao et al. 2019). Ren et al. (2015) integrated the accelerometer signal into a velocity signal, and then differentiated the velocity detector signal into acceleration, eliminating the phase difference between the two detectors. Additionally, Qin (2018) proposed a merging method using the derivative of geophone data in OBC dual-sensor seismic processing to obtain the scale conversion factor of the double inspection data. In terms of frequency matching, the working frequency band of the pressure detector and velocity detector is within 0–300 and 17–200 Hz (Liu et al. 2012). Therefore, the frequency band associated with the hydrophone data is wider than that of the geophone data. In the high frequency part, the geophone records are partially lost. In land seismic exploration, the spectral whitening method has been used to broaden the frequency band of the signal (Bian et al. 1986). Over the years, time–space variable spectral whitening (Fan 1995), wavelet spectral whitening (Chen 2000), and Hilbert spectral whitening methods (Wang 2012) have been developed. These methods are used in land seismic exploration and can achieve better results with regard to frequency band

broadening. In marine seismic exploration, the introduction of spectral whitening method in OBC seismic explorations can achieve the frequency matching of dual-sensor data (Quan and Han 2005). Subsequently, the Hilbert spectrum whitening method was applied to the high-resolution processing of marine seismic data (Yan 2018). Thus far, in marine seismic exploration, the frequency matching method of dual-sensor summation has been observed to generally adopt the spectral whitening method.

In an ideal situation, the ghost, using the opposite polarity hydrophone and geophone data, can be completely eliminated via the dual-sensor summation method. However, because of the complexity of the actual data, the ghost is rarely completely eliminated, leaving some residual interference. Moreover, because of the inevitable error and other interference during acquisition and processing, the sum results of dual-sensors often produce some noise. Currently, in marine streamer seismic exploration, the suppression of residual ghost after the synthesis of dual-sensor data is mainly performed via predictive deconvolution. However, after the emergence of submarine seismic exploration, no new methods have been proposed, meaning the predictive deconvolution method is still used to suppress residual ghost (Xue et al. 2013).

The key to suppressing ghost waves with dual-sensor summation technology is the matching of dual-sensor data. At present, several methods have been developed for amplitude and phase matching, while research on frequency matching methods has been limited and the results have been poor. Furthermore, in OBN seismic exploration, only few methods have been successful in suppressing residual ghost waves after dual-sensor summation. There is still room for improvement in the dual-sensor summation technology with regard to suppressing ghost waves. This study analyses the principles and characteristics of wavelet transform, and uses the unique advantages of wavelet transform to flexibly apply the wavelet spectrum whitening method to dual-sensor summation technology. In particular, the wavelet spectrum whitening method was used to match the frequency of the dual-sensor data, while the wavelet denoising method was proposed to suppress the ghost and noise remaining after dual-sensor summation in order to form a new set of processing procedures for OBN dual-sensor summation. The processing method includes the following steps: (1) matching the frequency, phase, and amplitude of the dual-sensor data with corresponding methods; (2) synthesising the matched dual-sensor data; and (3) adopting the nonlinear wavelet transform threshold method in the wavelet denoising method to eliminate residual ghost and noise in the sum data. The proposed method enhances the effect of double-sensor synthesis for de-ghosting, improves seismic resolution, and enhances the interpretation ability of processed seismic data.

Methods

Wavelet domain denoising

First, wavelet transform is used to decompose the signal by wavelet, then corresponding processing is applied, and finally the signal is reconstructed through inverse transformation in order to eliminate the signal. This process is called wavelet domain denoising, and its theoretical basis is wavelet transform.

Wavelet transform was proposed by Morlet, a French scientist, who introduced the concept to analyse local seismic waves (Morlet et al. 1982; Grossman and Morlet 1984).

Wavelets satisfy the condition:

$$\int_{-\infty}^{+\infty} \Psi(t)dt = 0 \tag{1}$$

With the $\Psi(t)$, a family of functions can be obtained after translation and scaling:

$$\Psi_{a,b}(t) = \frac{1}{\sqrt{|a|}}\Psi\left(\frac{t-b}{a}\right) \\ a,b \in R; a \neq 0 \tag{2}$$

where $\Psi(t)$ is the parent or base wavelet, a is the stretching factor (also called the scale factor), and b is the translation factor. Equation (2) produces the continuous wavelet generated by the base wavelet $\Psi(t)$. If the Fourier transform of $\Psi(t), \widehat{\Psi}(\omega)$ satisfies

$$C_\Psi = \int_{-\infty}^{+\infty} \frac{\left|\widehat{\Psi}(\omega)\right|^2}{|\omega|} d\omega < \infty \tag{3}$$

then, $\Psi(t)$ is an admissible wavelet, and Eq. (3) is an admissible condition.

If we let $\{\Psi_{a,b}\}$ be the wavelet function given by Eq. (2) for any function $f(t) = L^2(R)$, its wavelet transform is

$$W_f(a,b) = |a|^{-\frac{1}{2}} \int_{-\infty}^{+\infty} f(t)\Psi^*\left(\frac{t-b}{a}\right)dt \tag{4}$$

Equation (4) is called the continuous wavelet transform equation.

Meanwhile, signal processing adopts discrete wavelet transform as follows:

$$Wf_{m,n} = a_0^{-\frac{m}{2}} \int_{-\infty}^{+\infty} f(t)\Psi^*\left(a_0^{-m}t - nb_0\right)dt m,n \in \mathbf{Z} \tag{5}$$

Its reconstruction formula (inverse transformation formula) is

$$f(t) = \sum_{j\in Z} \int_{-\infty}^{+\infty} W_{2^{-j}}f(b)\left(2^j \widetilde{\psi}\left(2^j t - b\right)\right)db \tag{6}$$

The signal processing flow based on wavelet transform is shown in Fig. 3. Briefly, the initial signal s(t) is transformed to the wavelet domain via a discrete wavelet transform (DWT). Then, the transformed signal is processed in a wavelet domain. Finally, the processed signal is transformed via an inverse discrete wavelet transform to obtain the final result, that is, the signal ŝ(t).

Since it was first proposed, the wavelet transform theory has experienced rapid development, in which its application in different fields is continuously expanding. In terms of noise removal, the wavelet transform theory has achieved meaningful results. The success of the wavelet denoising method is mainly the result of the following characteristics of wavelet transform:

(1) Multi-resolution: The multi-resolution method is beneficial for obtaining a detailed characterization of the non-stationary characteristics of the signal, including the edge, abrupt change, and breakpoint.
(2) De-correlation: Wavelet transform undergoes a de-correlation process for the processed signal. After wavelet transform, the noise exhibits a whitening trend, thereby providing a better denoising effect.
(3) Flexibility of base selection: Wavelet transform has numerous wavelet bases, and the corresponding wavelet generating function can be flexibly selected according to the characteristics of different signals in order to obtain the best processing results.

There are many wavelet denoising methods, among which the threshold method of nonlinear wavelet transform is common and effective (Donoho 1995; Donoho and Johnstone 1995). The specific steps of this method are described here. First, the signal is decomposed by wavelet transform. Then, as the noise signal is mostly contained in the high frequency data, the threshold form (hard-threshold or soft-threshold) can be used to process the decomposed wavelet coefficient. Finally, the noise can be eliminated via wavelet reconstruction.

According to the characteristics of the signal, a soft-threshold value was adopted in this study to de-noise the dual-sensor sum signal. The specific steps are as follows:

(1) The 'SYM4' wavelet and the scale N = 10 were selected (Yan and Zhou 2012) to perform a one-dimensional multi-scale transformation of the dual-sensor signal, and the parameter matrices of C and L were obtained. Parameter C is composed of [cA10,cD10,cD9,cD8…
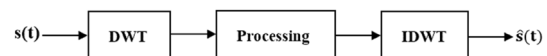

Fig. 3 Signal processing block diagram based on wavelet transform

cD1], where cA10 represents the low frequency coefficient, and cD10,cD9,cD8…,cD1 represent the high frequency coefficients at various scales. L consists of [length of cAj, length of cDj…, length of X].

(2) Without changing the parameter L, soft-threshold processing is conducted on coefficient matrix C to form the matrix CC which is a matrix after soft threshold processing. The threshold processing process is as follows: the first five elements in C are copied to corresponding positions in CC. Then the threshold (THRES) is determined and the remaining elements in C are traversed. Note that when C(I) is less than or equal to THRES, CC(I) is set to zero; when C(I) is greater than THRES, CC(I) = C(I)-THRES; and when C(I) is less than -THRES, CC(I) = C(I) + THRES. For this process, the selection of the THRES is key. The appropriate threshold corresponding to different signals is different depending on the specific situation.

(3) The parameter matrices CC and L are used for signal reconstruction under 'sym4' to obtain the denoised signal, wherein the residual ghost and other noise are eliminated. The flowchart of wavelet denoising is shown in Fig. 4.

Wavelet spectral whitening method

Currently, the frequency matching of dual-sensor summation processing mainly employs the spectral whitening method. However, the spectral whitening method uses the Fourier transform method to transform the time and frequency domains, which prevents the effective analysis of the local frequency characteristics of data. To overcome this issue, Chen and Zhou (2000) proposed combining wavelet transform and the wavelet spectral whitening method to improve the resolution of terrestrial seismic data. Wavelet transform can adjust the width of the time window according to different frequency components of the signal, allowing the signal to be described more effectively, which is more conducive to signal analysis and processing. Therefore, in this study, wavelet spectral whitening was introduced into the frequency match processing of the dual-sensor summation technology of OBN seismic data in order to match the frequencies of the geophone and hydrophone data.

The process of frequency matching dual-sensor data using the wavelet spectral whitening method is shown in Fig. 5. First, discrete wavelet transform (decomposition) is performed on the geophone signal to calculate the decomposition signals of different scales. Then, spectral whitening is applied to the scale signal to compensate for the missing high-frequency portion. Finally, the compensated scale signal is inversely transformed (reconstructed) to obtain the hydrophone signal after frequency matching.

The basic steps of spectral whitening are as follows (Bian et al. 1986):

(1) Conduct narrow-band pass filtering:

Suppose a seismic record is $x(n\Delta t)$, where n is the serial number of sampling points and Δt is the sampling interval. The Fourier transformation of $x(n\Delta t)$ gives the amplitude spectrum
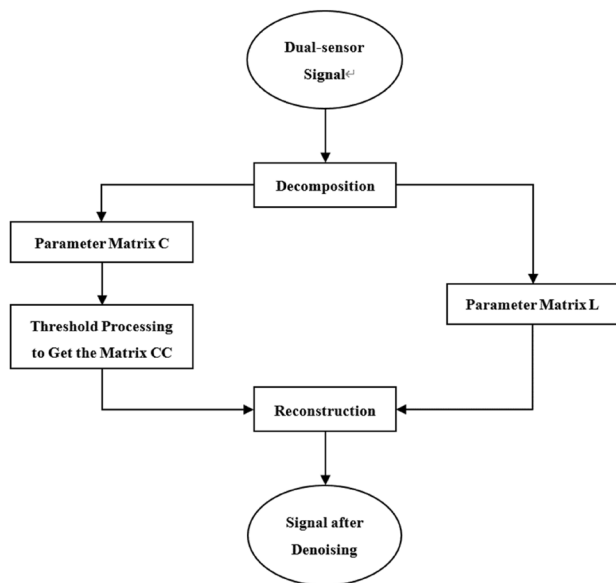

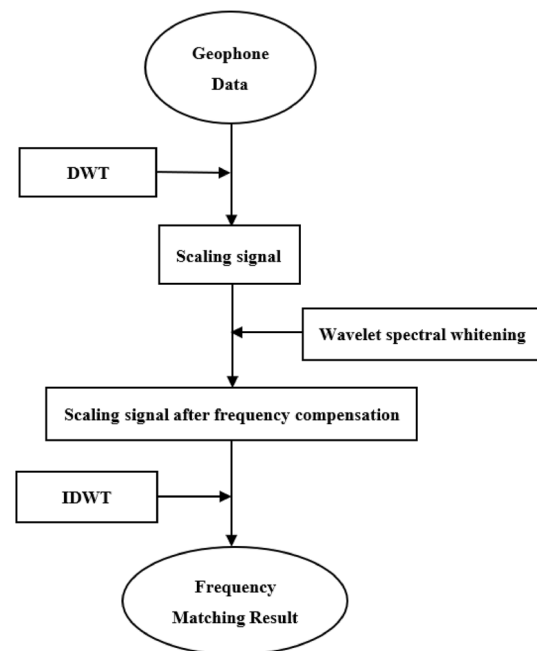Fig. 4 Wavelet denoising flowchart of dual-sensor signals

Fig. 5 Frequency matching flowchart of the wavelet spectral whitening method

$$\widehat{X}(m\Delta f) = \sum_{n=0}^{N-1} x(n\Delta t)e^{-i2\pi m\Delta f \cdot n\Delta t} \qquad (7)$$

We can then compute $\widehat{X}(m\Delta f)$ using frequency division narrow-band pass filtering

$$\widehat{X_k}(m\Delta f) = \widehat{X}(m\Delta f) \cdot H_k(m\Delta f) \; k = 1, 2, \ldots, K \qquad (8)$$

where $H_k(m\Delta f)$ is a bandpass filter and K is the number of bandpass filters.

Next, we apply an inverse Fourier transformation to $\widehat{X_k}(m\Delta f)$ to compute k records after computing the frequency division:

$$x_k(n\Delta t) = \sum_{m=0}^{M} \widehat{X_k}(m\Delta f)e^{i2\pi m\Delta f \cdot n\Delta t} \qquad (9)$$

(2) Determine time-varying gain:

Each $x_k(n\Delta t)$ is divided into several time windows, in which the root mean square value of each time window is calculated using

$$A_{kj} = \sqrt{\frac{1}{T+1}\sum_{n=r}^{r+T} x_k^2(n\Delta t)} \qquad (10)$$

where A_{kj} is the *k-th* frequency division record and the root mean square value of the amplitude in the *j-th* time window. In addition, j is the time window number, r is the time window start time, and T is the time window length.

The expression $x_{kj}(n\Delta t)$ can be denoted as the *k*-th frequency division record in the *j*-th time window to obtain the gain method as follows:

$$\bar{x}_{kj}(n\Delta t) = \frac{x_{kj}(n\Delta t)}{A_{kj}} \cdot C \qquad (11)$$

where C is a constant.

The time-varying gain is then applied to the signals in each band and added,

$$\bar{x}(n\Delta t) = \sum_{k=1}^{K} \bar{x}_k(n\Delta t) \qquad (12)$$

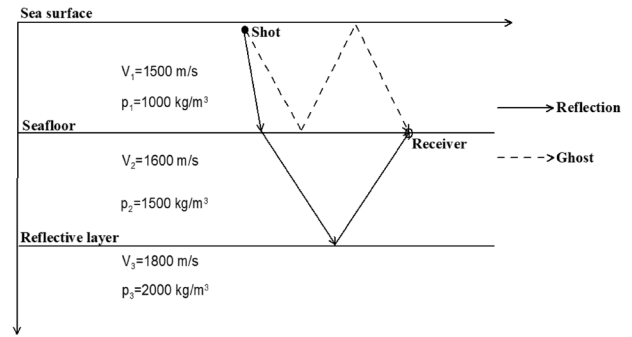where $\bar{x}(n\Delta t)$ is the result of spectral whitening.

Fig. 7 Ocean-bottom nodes (OBN) model

Dual-sensor summation technology process

During the dual-sensor summation process, frequency matching uses the wavelet spectrum whitening method proposed in this article, whereas phase and amplitude matching employ single-channel Wiener filtering (Tong et al. 2012) and the similarity coefficient method (Tao et al. 2019). Meanwhile, residual ghost suppression utilizes the wavelet denoising method. Together, a complete dual-sensor summation processing system is established (Fig. 6). It is worth mentioning that it is relatively easy to match the wideband data to the narrowband data. But this study matches the frequency of the geophone data to be consistent with the hydrophone data. Because this processing has three advantages. First, the amplitude matching and phase matching methods both match the land geophone data to the hydrophone data, so the frequency matching also matches geophone data (narrowband data) with the hydrophone data (wideband data), which can make the three matching processes remain the same. Second, matching the narrow-band data with the wide-band data can compensate for the loss of the high-frequency part of the land survey data due to factors such as the nature of the detector and the external environment. Third, matching the narrow-band data with the wide-band data to broaden the frequency band can narrow the in-phase axis in the seismic record, thereby improving the signal resolution.

Model data testing

Synthetic seismic record

According to the geometric relationships, the OBN horizontal layered synthetic seismic record, as shown in Fig. 7, was established. The first layer is a water layer, wherein the water depth is 100 m, the v_p is 1500 m/s, and ρ is 1000 kg/m³. The second

Fig. 6 Process flowchart of the dual-sensor summation method
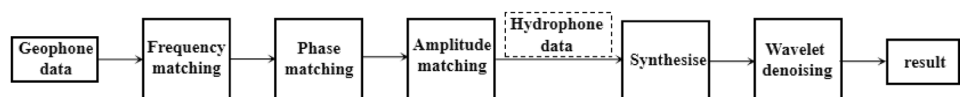
layer is dielectric with a thickness of 300 m, a v_p of 1600 m/s, and a ρ of 1500 kg/ m^3. The third layer is a uniform infinite space, with a v_p of 1800 m/s and a ρ of 2000 kg/m^3. The gun point is located at the sea surface (500, 5), and the receiving end exists at the seabed interface. There are 101 channels in total, with a spacing of 100 m, a minimum offset of 0 m and a sampling interval of 1 ms. A Riker wavelet with a dominant frequency of 60 Hz was used to synthesize the hydrophone record, and that with a dominant frequency of 30 Hz was used to synthesize the geophone record in order to simulate the difference between the hydrophone and geophone records in the frequency band.

Wavelet spectral whitening was used to conduct frequency matching on the dual-sensor data. Figure 8 shows the spectrum diagram of the 52nd track record before and after frequency matching. Figure 8a reveals an obvious difference in the frequency band range between the hydrophone and geophone records. In the low frequency range (0–60 Hz), both records contain data, whereas in the high frequency range (60–110 Hz), geophone data is missing. Thus, frequency matching must be conducted to establish a consistent frequency band range for both records. The wavelet spectrum whitening method is used to match the frequency of the geophone data to ensure that its frequency band range is consistent with that of the hydrophone data. It can be seen that the high frequency part of the geophone data has been balanced, while the low frequency part has been retained.

Figure 9 shows the geophone records before and after frequency matching. It shows that the range of the geophone records significantly narrowed after frequency matching, thereby indicating that the resolution improved; this result is consistent with the hydrophone records.

Figure 10 shows the dual-sensor summation process. Figure 10a reveals the geophone records after frequency,

phase, and amplitude matching. At this stage, the geophone and hydrophone records demonstrated consistent frequencies, phases, and amplitudes. Subsequently, the hydrophone records are added to obtain the dual-sensor summation record (c). At this point, the ghost was basically eliminated and the effective wave (direct and reflected waves) was retained. However, some ghost remained. Thus, the wavelet denoising method was adopted to remove the residual ghost (noise), completely suppressing the ghost (d). The results show that adding the wavelet transform to the dual-sensor summation process produces good results.

Figure 11 shows the comparison of the dual-sensor summation results after frequency matching using wavelet spectral whitening and using traditional spectral whitening methods. The results show that the results after wavelet spectral whitening were significantly better than those after traditional spectral whitening, indicating the former ghost suppression method is more thorough, as there is less remaining residue. Thus, the frequency matching effect of wavelet spectrum whitening should be used in future dual-sensor syntheses to suppress the ghost.

Forward model

Figure 12 shows the established OBN horizontal layered model, with a length of 10,000 m. The first layer in the model is a water layer, with a depth of 100 m, a wave velocity of 1500 m/s, and a ρ of 1000 kg/m^3. The second layer is a 500 m thick medium layer, with a v_P of 1800 m/s, a v_S of 850 m/s, and a ρ of 1800 kg/m^3. The third layer is a 3000 m thick medium layer, with a v_P of 2300 m/s, a v_S of 1200 m/s, and a ρ of 2350 kg/m^3. The fourth layer is infinite space, with a v_P of 3000 m/s, a v_S of 1450 m/s, and a ρ of 2350 kg/m^3. In this model, the shot and receiving points are located
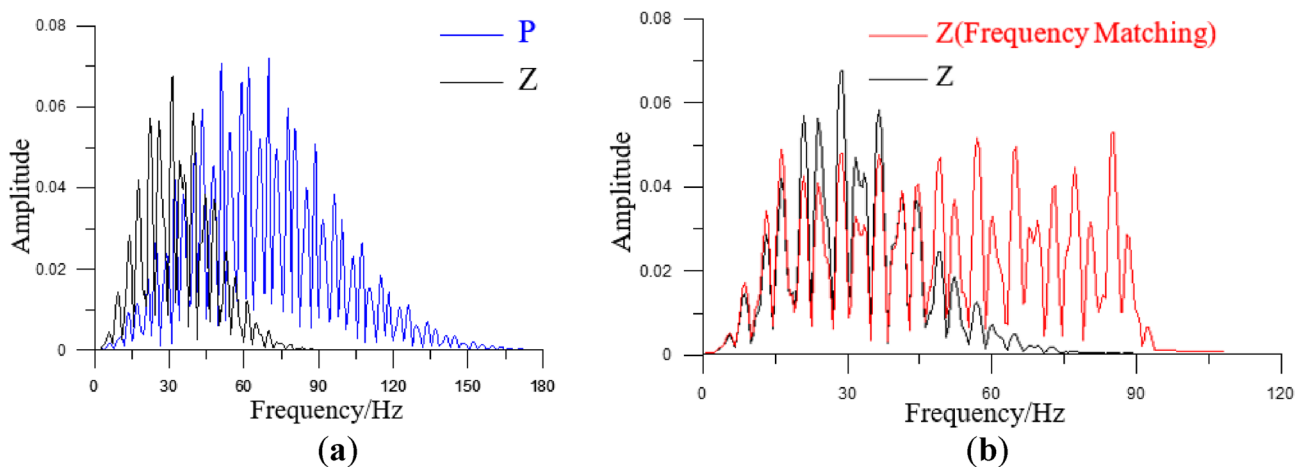
Fig. 8 Spectrum diagram of dual-sensor data. **a** Spectral comparison of P and Z components; **b** Spectrum comparison before (in black) and after(in red) wavelet spectrum whitening
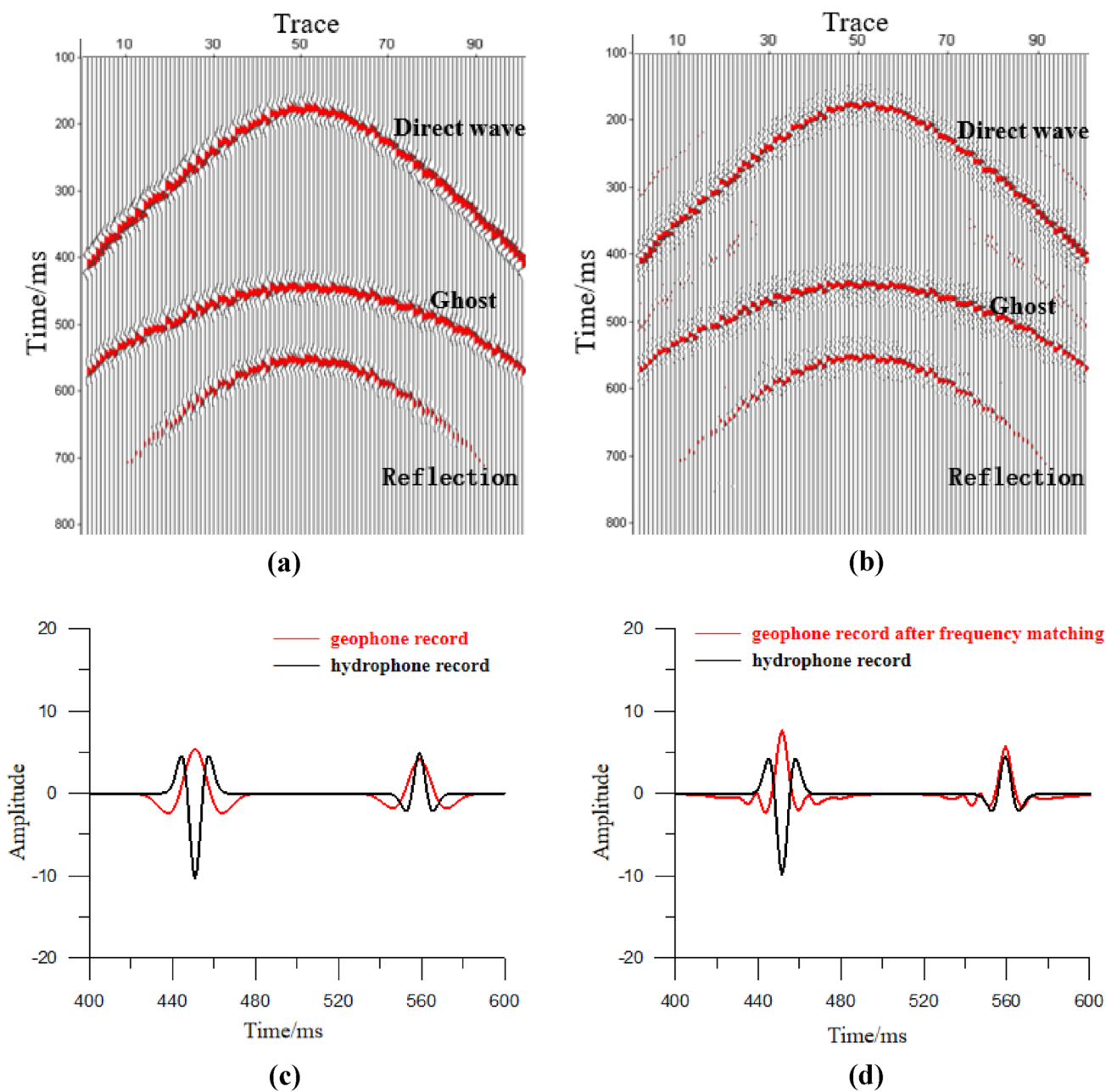
Fig. 9 Seismic records before and after frequency matching. **a** Geophone records, **b** geophone records after frequency matching, **c** comparison of an original hydrophone record with geophone record, and **d** comparison of a hydrophone record with geophone record after frequency matching

at the sea surface (5000, 5), and the sea bottom, respectively. In total, there are 101 channels, with a spacing of 100 m, a minimum offset of 0 m, and a sampling interval of 1 ms. The frequency band of the hydrophone data is generally wider than that of the geophone data. In the high frequency part, geophone records are partially lost due to factors such as the nature of the geophone and the external environment. Therefore, when the seismic record is generated using the acoustic wave equation, the wavelet dominant frequencies of hydrophone and geophone records are set to 60 and 30 Hz,

respectively, to simulate the lack of high-frequency part in the actual geophone record.

Figure 13 shows the spectrum diagram of the 53rd track record before and after frequency matching. The results reveal that there is an obvious difference in the frequency band range between the hydrophone and geophone records. Specifically, in the low frequency range (0–40 Hz), both records have sufficient data, but in the high frequency range (40–70 Hz), geophone data is missing and requires frequency matching to make both ranges consistent. The high
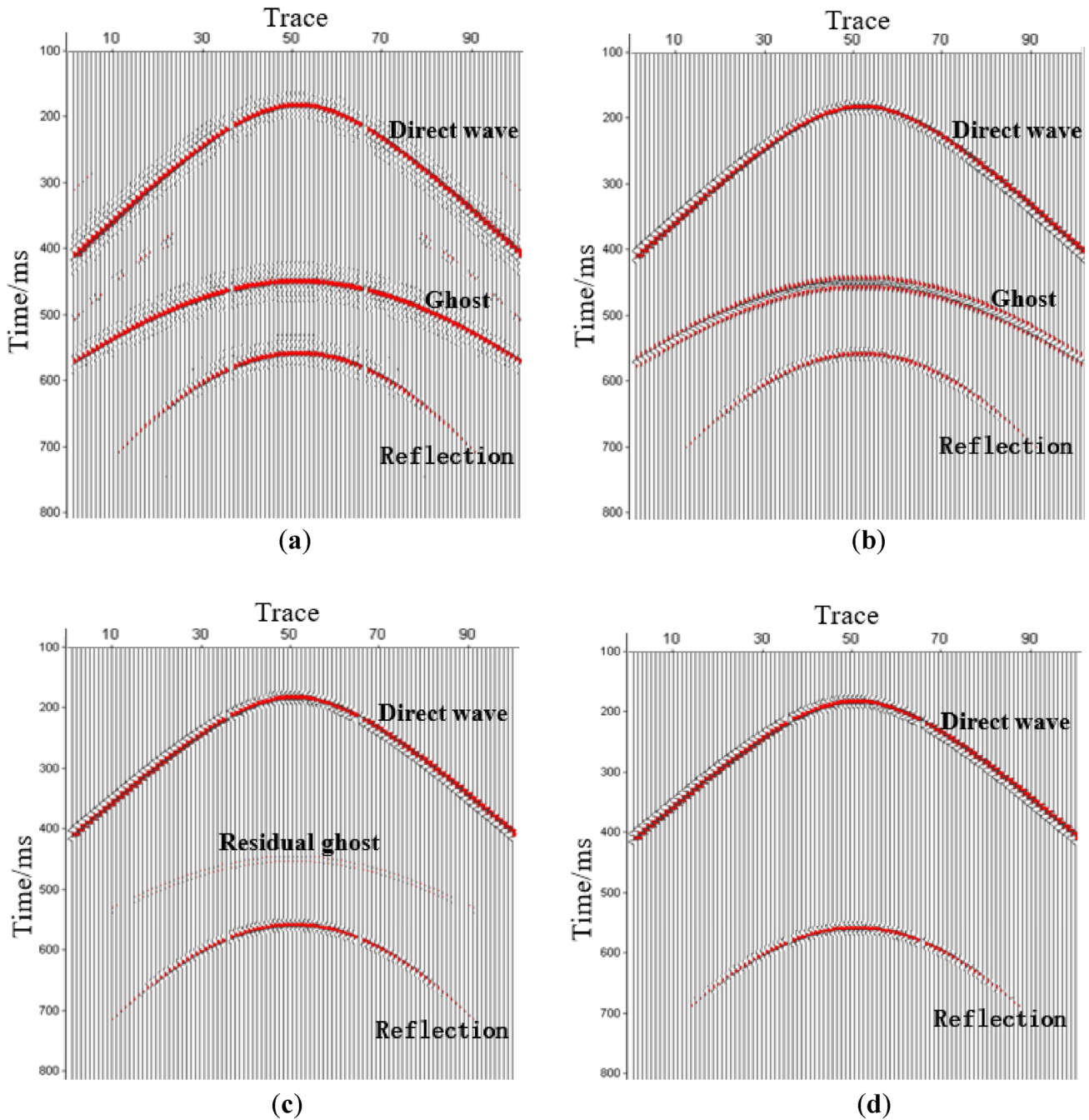
Fig. 10 Dual-sensor summation process. **a** Geophone records after frequency, phase, and amplitude matching; **b** hydrophone records; **c** dual-sensor summation records; and **d** denoised dual-sensor summation record

frequency part of the geophone record is completed using the wavelet whitening method. These results indicate that the wavelet whitening method can effectively match the frequencies of the dual-sensor data.

Figure 14 shows the efficacy of the dual-sensor summation process, where Fig. 14a is the original geophone record, and Fig. 14b is the geophone record after frequency phase and amplitude matching. The results show

that the matching process inevitably creates some noise (blue box). Figure 14c shows the dual-sensor summation record obtained by combining the hydrophone and geophone records, which reveals that most of the ghost has been eliminated, direct and reflected waves are retained. In addition, the shallow and deep reflected waves hidden in the ghost are revealed by removing the ghost. However, there exists some residual ghost and noise. Figure 14d
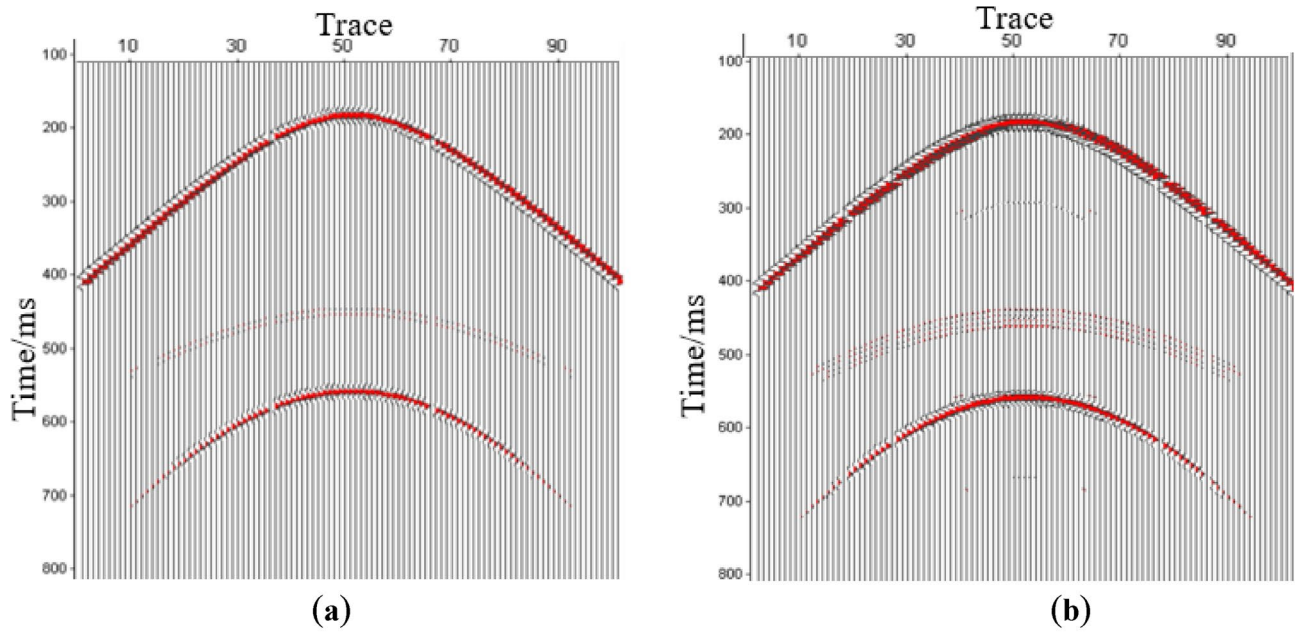
Fig. 11 Comparison of frequency matching effects. **a** The results of the dual-sensor summation of the wavelet spectrum whitening method, and **b** dual-sensor summation results of spectrum whitening

shows the wavelet denoising results. After removing the residual ghost and noise, the profile became cleaner and the effective wave was relatively strengthened. This reveals that the dual-sensor summation processing with wavelet transform produces good results, significantly improving the signal-to-noise ratio of the dual-sensor summation data.

Figure 15 shows the 53rd single track record. The conclusion consistent with Fig. 14 can be obtained.
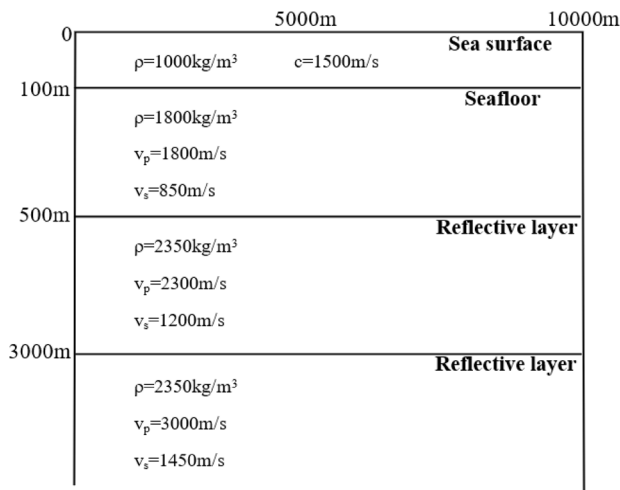

Fig. 12 Forward ocean-bottom nodes (OBN) model

Application examples

In this study, the hydrophone and geophone records of submarine node seismic survey data were completely processed. Figure 16 shows the spectrum diagram of the single-channel record before and after frequency matching. The results show that there is an obvious difference between the frequency band ranges of the hydrophone and geophone records. In the low frequency range (0–80 Hz), both records have sufficient data, while in the high frequency range (80–170 Hz), the geophone and hydrophone data differ greatly as a result of missing information. Therefore, frequency matching must be performed to make the frequency bands consistent. The high frequency part of the geophone record is completed using the wavelet whitening method, making its range consistent with that of the hydrophone record. Overall, it can be seen that the wavelet whitening method can be effectively used to match the frequencies of the dual-sensor data.

Figure 17 shows the comparison before and after the dual-sensor summation, wherein panel (a) is the hydrophone record and (b) is the dual-sensor summation record. After matching, the water and geophone records were consistent in frequency, amplitude, and phase and the ghost can be eliminated via dual-sensor summation. It can be seen that in the black box, some of the events (ghost) visible to the naked eye have been eliminated, indicating effective ghost suppression.

The average amplitude spectra of the ranges circled by the black box in Fig. 17a and b (i.e. the 550–600 channel and
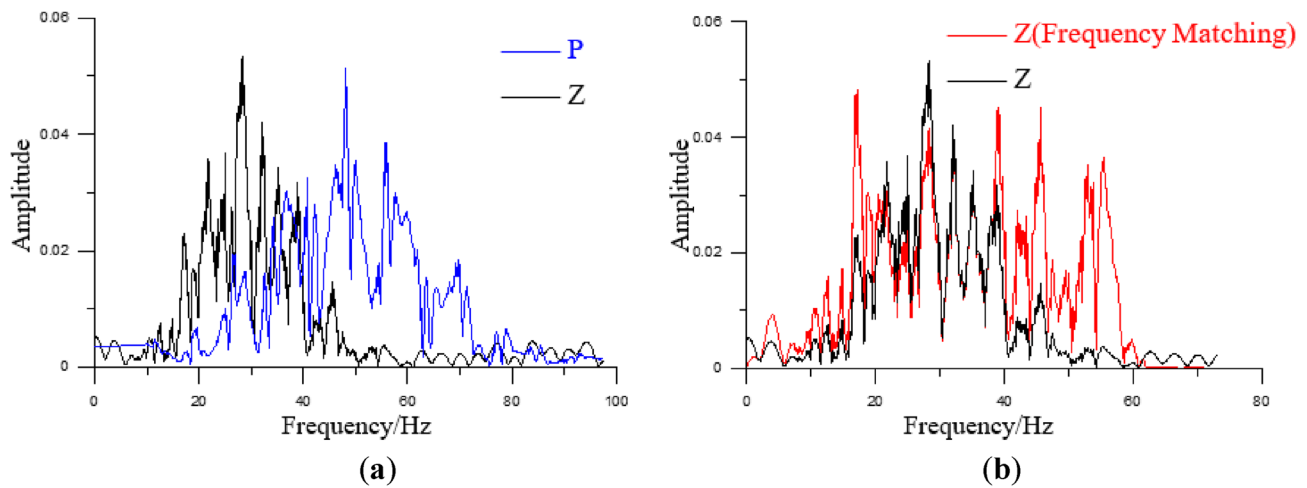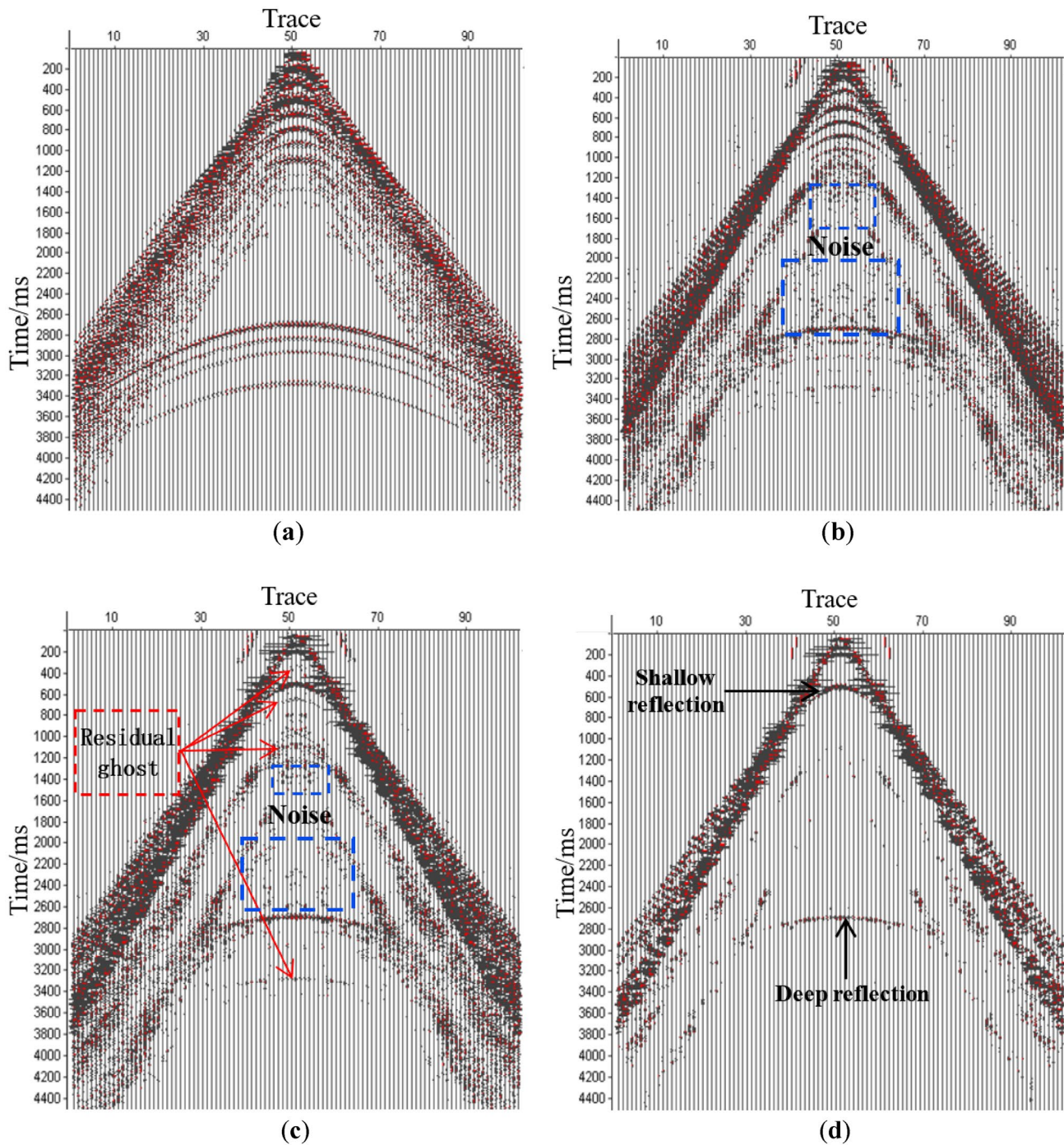
Fig. 13 Spectrum diagram **a** Spectral comparison of P and Z components; **b** spectrum comparison before and after wavelet spectrum whitening

1000–2000 ms time window) were calculated and compared, as shown in Fig. 18. Figure 18 shows the position marked by the blue circle, which demonstrates that the amplitude spectrum is significantly elevated, indicating that the notch effect and signal loss caused by the ghost wave is suppressed and avoided, respectively. The notch effect caused by the ghost was weakened and the spectra at some positions increased after suppressing the ghost wave via dual-sensor summation, implying that the dual-sensor summation has an observable effect.

Conclusions

In this study, wavelet transform was incorporated into the calculation of dual-sensor summation technology of OBN seismic exploration data, and a dual-sensor technology process was proposed for the OBN dual-sensor data. First, the wavelet spectral whitening method was introduced to match the frequencies of the dual-sensor data to eliminate differences in the frequencies of the hydrophone and geophone data. Then, the phase and amplitude of the dual-sensor data were matched using the similarity coefficient method and the single-channel Wiener filter method, respectively, making the hydrophone and geophone data consistent. Next, both records were combined to suppress the ghost. Finally, the nonlinear wavelet transform threshold method of the wavelet denoising method was used to further suppress the residual ghost and eliminate noise caused by the dual-sensor summation process, producing the final processing result. By establishing an OBN model for a trial calculation, it was verified that the proposed process produces improved processing results. The findings of this study provide a suitable method for calculating OBN seismic exploration data. However, for larger data, the computational efficiency will decrease because of the addition of wavelet transform. Thus, the algorithm needs to be optimized further.

Fig. 14 Dual-sensor summation processing. **a** Geophone records; **b** geophone records after frequency, phase, and amplitude matching; **c** dual-sensor summation record; and **d** denoised dual-sensor summation record

(a)

(b)

(c)

(d)
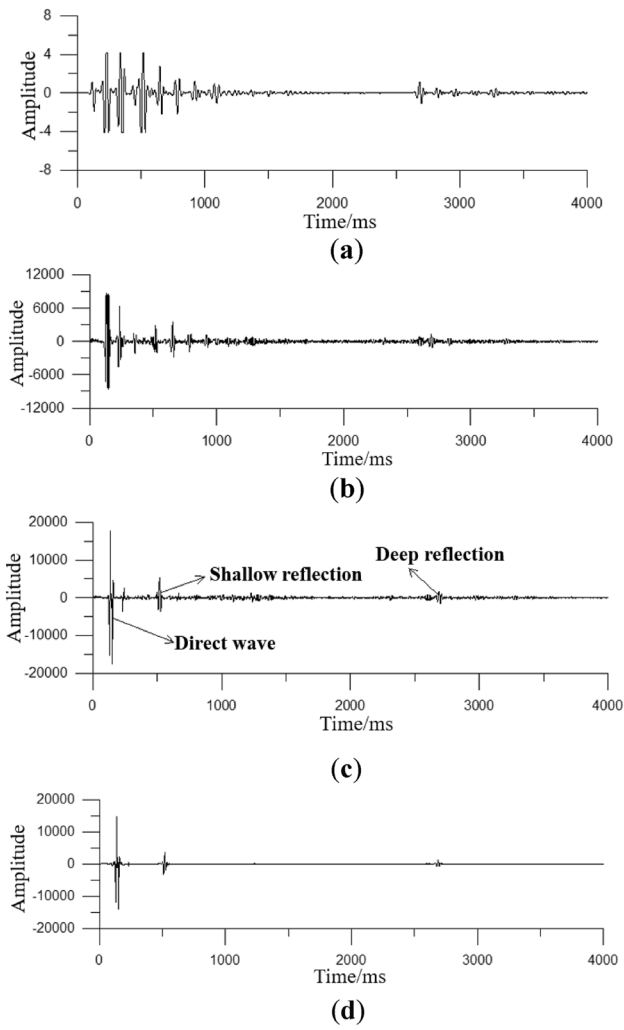
Fig. 15 Single-channel record processing by dual-sensor summation **a** Geophone records; **b** geophone records after frequency, phase, and amplitude matching; **c** dual-sensor summation records; and **d** denoised dual-sensor summation record

(a)

(b)
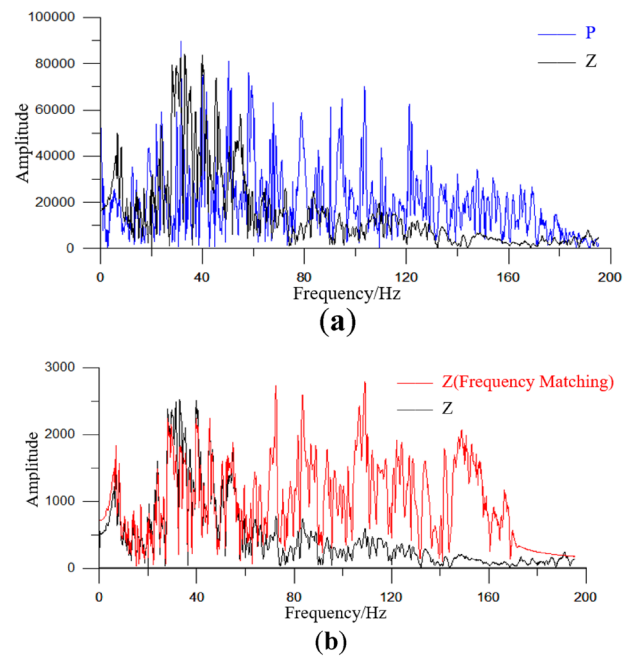
Fig. 16 **a** Spectral comparison of P and Z components; **b** spectral comparison before and after wavelet spectrum whitening

(a) Hydrophone record

(b) Dual-sensor summation result
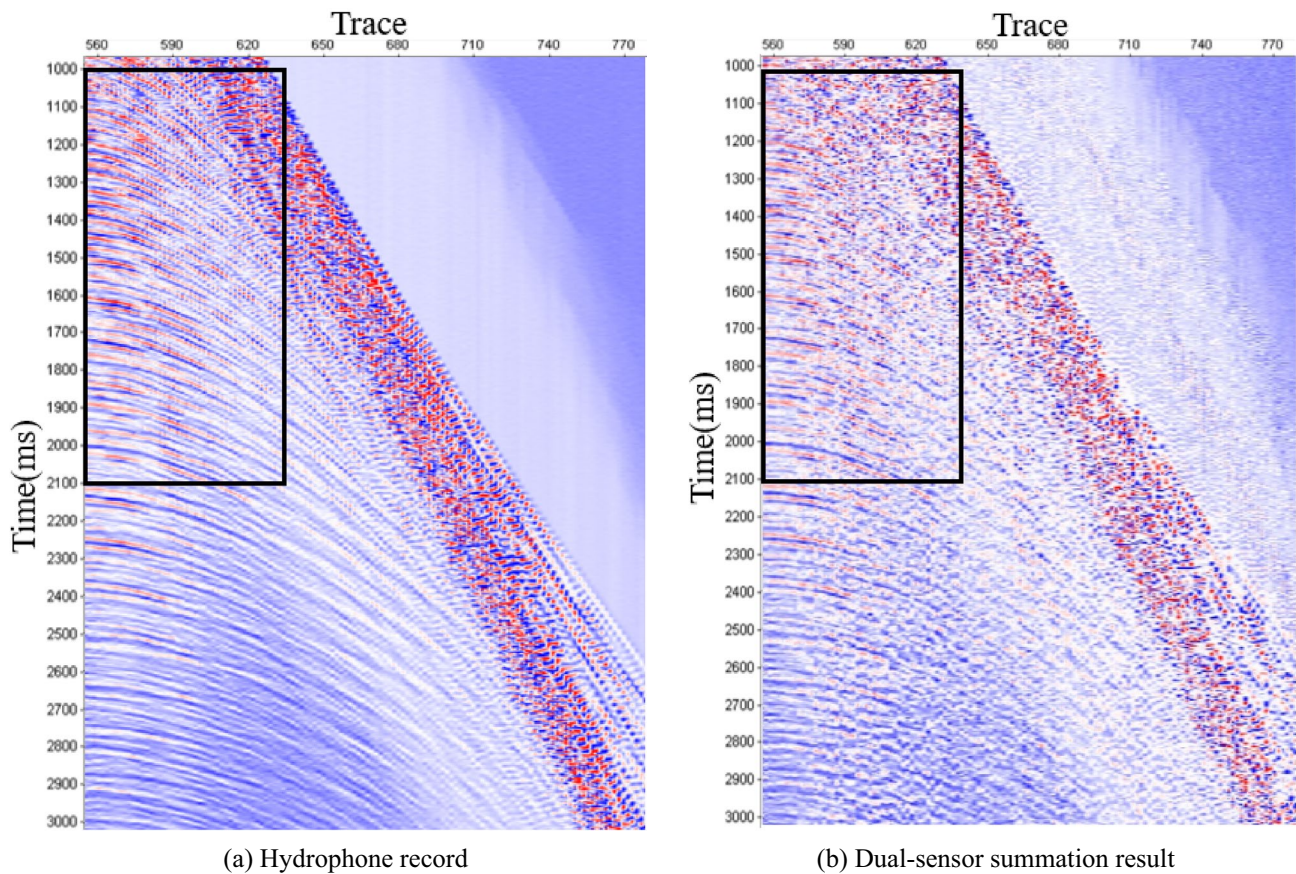
Fig. 17 Comparison of the dual-sensor summation results
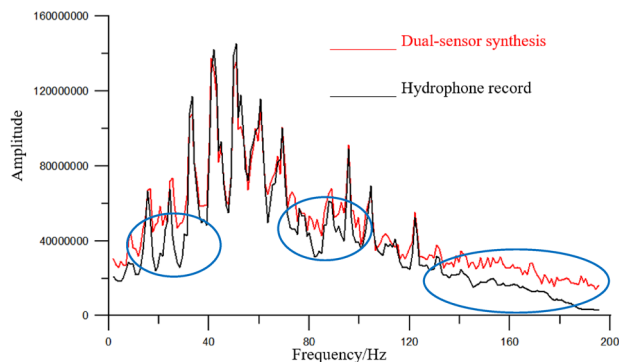
Fig. 18 Comparison of average amplitude spectra

Author contributions All authors contributed to the research in the paper. Conceptualization: SS and QCL; Methodology: ZXW and GP; Formal analysis and investigation: ZXW; Writing—original draft preparation: ZXW and GP; Writing—review and editing: SS and QCL; Supervision: QCL All authors have read and agreed to the published version of the manuscript.

Declarations

Conflict of interest The authors declare no conflict of interest.

References

Ball V, Corrigan D (1996) Dual-sensor summation of noisy ocean-bottom data//66th Annual International Meeting. SEG Expand Abs. https://doi.org/10.1190/1.1826622

Barr FJ, Sanders JI (1989) Attenuation of water column reverberation using pressure and velocity detectors in a wager-bottom cabled. Expand Abs 59st SEG Mtg. https://doi.org/10.1190/1.1889557

Bian GZ, Zhang LQ (1986) Spectral whitening of seismic data. Geophys Prospect Petrol 02:26–33

Chen CR, Zhou XX (2000) Improving resolution of seismic data using wavelet spectrum whitening. Oil Geophys Prospect 35:703–709. https://doi.org/10.13810/j.cnki.issn.1000-7210.2000.06.003

Donoho DL (1995) Denoising by soft-thresholding. IEEE Trans Inf 3:613–627. https://doi.org/10.1109/18.382009

Donoho DL, Johnstone IM (1995) Adapting to unknown smoothness via wavelet shrinkage. J Am Stat Assoc 90(432):1200–1224. https://doi.org/10.1080/01621459.1995.10476626

Dragoset B, Barr FJ (1994) Ocean-bottom cable dual-sensor scaling. SEG Tech Program Expand Admin. https://doi.org/10.1190/1.1932022

Fan XD, Zeng H, Liu YQ (1995) Time-space variant spectrum whitening of seismic data. Oil Geophys Prospect 30(4):550–5572

Gao SW, Zhao B, Gao X, Zhu KH, Li GF (2015) A method for OBC dual-sensor data matching. Oil Geophys Prospect 50:29–32. https://doi.org/10.13810/j.cnki.issn.1000-7210.2015.01.005

Gao SW, Zhou XY, Cai JM et al (2001) Surface consistent phase correction of reflected waves. Petrol Geophys Explor 36(4):480–487. https://doi.org/10.3321/j.issn:1000-7210.2001.04.014

Grossmann A, Morlet J (1984) Decomposition of Hardy functions into square integrable wavelets of constant shape. SIAM J Math Anal 15(4):723–736. https://doi.org/10.1137/0515056

Hoffe BH, Lines LR, Cary PW (2000) Applications of OBC recording. Leading Edge 19(4):382–391. https://doi.org/10.1190/1.1438616

Jiao J, Trickett S, Link B (1998) Ocean-bottom-cable dual-sensor summation: a robust approach. CSPG Special Publications.

Levy S, Oldenburg DW (1987) Automatic phase correction of common-midpoint stacked data. Geophysics 52(1):51–59. https://doi.org/10.1190/1.1442240

Liu ZD, Lu QT, Dong SX, Chen MC (2012) Research on velocity and acceleration geophones and their acquired information. Appl Geophys 9(2):149–158. https://doi.org/10.1007/s11770-012-0324-6

Morlet J, Arens G, Fourgeau E, Giard D (1982) Wave propagation and sampling theory—Part II: sampling theory and complex waves. Geophysics 47(2):222–236. https://doi.org/10.1190/1.1441329

Paffenholz J, Barr FJ (1995) An improved method for deriving water-bottom reflectivi-tiesfor processing dual-sensor ocean-bottom cable data. SEG Expand Abs. https://doi.org/10.1190/1.1887432

Qin N (2018) Merging method using the derivative of geophone data in OBC dual-sensor seismic processing. Prog Geophys (in Chinese) 33(3):1269–1273. https://doi.org/10.6038/pg2018BB0268

Quan HY, Han LQ (2005) Using OBC dual-receiver to suppress reverberation of water column. Oil Geophys Prospect 40:7–12. https://doi.org/10.13810/j.cnki.issn.1000-7210.2005.01.007

Ren LG, Zhang GD, Yang DK et al (2015) Analysis and application of phase different between velocity geophone and piezoelectric geophone. Prog Geophys (in Chinese) 30(1):0454–0459. https://doi.org/10.6038/pg20150167

Song YL, Zhang J, Yang HC (2004) Explored and receives problem of the oil gas seismic exploration in amphibious area. Prog Geophys 19(2):424–430. https://doi.org/10.3969/j.issn.1004-2903.2004.02.033

Tao J, Li B, Zhou XW (2019) Phase matching technology and its application in suppressing OBN reverberation. Geophys Geochem Explor 43:380–385. https://doi.org/10.11720/wtyht.2019.0007

Tong SY, Xiang F, Wang DK (2012) Suppression of reverberation by the technology of dual-sensor merger based on wiener filtering. Mar Geol Front 28:46–52. https://doi.org/10.16028/j.1009-2722.2012.10.005

Wang J (2012) High resolution seismic processing based on whitening of Hilbert spectrum. J China Coal Soc 37(01):50–54. https://doi.org/10.13225/j.cnki.jccs.2012.01.001

Xue WZ, Wang SR, Yang XY, Liu ZhH, Su Y (2013) OBC dual-sensor data processing on the Echos processing system. Oil Geophys Prospect 48:23–26. https://doi.org/10.13810/j.cnki.issn.1000-7210.2013.s1.005

Yan Q, Zhou DM (2012) The selection of basis functions of wavelet transform in signal analysis. Comput Telecommun 3:49–50. https://doi.org/10.15966/j.cnki.dnydx.2012.03.014

Yan ZH, Fang G, Xu HN, Liu J, Shi J, Pan J, Wang JQ (2018) The application of Hilbert spectral whitening method to high resolution processing of marine seismic data. Mar Geol Quat Geol 38(04):212–220. https://doi.org/10.16562/j.cnki.0256-1492.2018.04.019

Zhou XY (1989) Constant phase correction. Petrol Geophys Explor 24(2):119–129

Publisher's Note Springer Nature remains neutral with regard to jurisdictional claims in published maps and institutional affiliations.